Open loop liquid crystal adaptive optics systems: progresses and results

Cao Zhaoliang, Mu Quanquan, Xu Huanyu, Zhang Peiguang, Yao Lishuang, Xuan Li

(State Key Laboratory of Applied Optics, Changchun Institute of Optics, Fine Mechanics and Physics, Chinese Academy of Sciences, Changchun 130033, China)

Abstract: Liquid crystal wavefront corrector (LCWFC) is one of the most attractive wavefront correction devices for adaptive optics system. The main disadvantages for conventional nematic LCWFC are polarization dependence and narrow working waveband. A polarized beam splitter (PBS) based open loop optical design and an optimized energy splitting method was used to overcome these problems respectively. The results indicate that the open loop configuration is suitable for LCWFC and the novel energy splitting method can significantly improve the detection capability of the liquid crystal adaptive optics system.

Key words: open loop; adaptive optics; liquid crystal wavefront corrector

CLC number: O437 **Document code:** A **DOI:** 10.3788/IRLA201645.0402002

开环液晶自适应光学系统:研究进展和结果

曹召良,穆全全,徐焕宇,张佩光,姚丽双,宣 丽

(中国科学院长春光学精密机械与物理研究所 应用光学国家重点实验室,吉林 长春 130033)

摘 要: 对于自适应光学系统,液晶波前校正器是一个非常有前景的波前校正器件。传统的向列相液晶波前校正器的主要缺点是偏振依赖和工作波段窄。采用了基于偏振分束器的开环光路设计和优化的能量分割方法来分别解决上述问题。结果显示,开环光路非常适合于液晶波前校正器,且新颖的能量分割方法显著提高了液晶自适应光学系统的探测能力。

关键词: 开环; 自适应光学; 液晶波前校正器

收稿日期:2015-08-09; **修订日期:**2015-09-09

基金项目:国家自然科学基金(11174274,11174279)

作者简介:曹召良(1974-),男,研究员,博士,研究方向为液晶自适应光学和衍射光学。Email: caozlok@ciomp.ac.cn

0 Introduction

Liquid crystal wavefront correctors (LCWFCs), which are used to meet the spatial resolution demand of large aperture telescopes, have been widely investigated[1-6]. However, compared with deformable mirrors, LCWFC has the disadvantages of low energy utilization and slow response. To correct atmospheric turbulence, the response speed of the liquid crystal (LC) should be extremely high. To improve the frame rate of the LCWFC, ferroelectric and dual frequency LC materials were used by others[3,7]. However, due to its high voltage requirement and the complexity of the control method, the dual frequency LCWFC has difficulty in handling millions of active elements. The binary phase modulation of ferroelectric LCs limits their effectiveness. Consequently, our group mainly investigated the LCWFC with conventional nematic LC materials. With the LC molecule design [8] and optimal LC device parameter selection[9-10], the response time of the LCWFC can be down to sub-millisecond.

Another key problem is its low light energy utilization efficiency. Due to its polarization dependence, only polarized light, whose polarization direction is parallel to the LC alignment direction, can be modulated by the LCWFC. For conventional LCWFCs, a polarizer is used in adaptive optics system to generate the polarized light. Due to the use of polarizer, there will be more than 50% energy loss. Some special techniques have been used to solve this problem, but it makes the device hard to manufacture and expensive[11-12]. Aside from polarization dependence, the narrow working spectral range of liquid crystal adaptive optics systems (LC AOSs) contributes to the energy loss. Recently, Stockley demonstrated that non-dispersive LCWFCs can be obtained by utilizing chiral smectic ferroelectric liquid crystals[13]. However, this kind of LCWFC has limitations of low quantified phase level, circular polarization incident light, and amplitude modulation.

An overall work of our group onto the solution of the low energy utilization ratio will be introduced in this paper. Based on open loop control technique, the optimal optical system designs are performed to improve the energy utilization ratio of the liquid crystal adaptive optics system (LC AOS).

1 Optimal optical design to avoid the polarization energy loss

The conventional LC AOSs, as shown in Fig.1 (a), are controlled with closed loop mode[14-15]. At this mode, the wavefront sensor (WFS) is followed to the LCWFC and the correction error can be detected. However, as a polarizer is used, 50% energy loss is caused. To avoid this energy loss, a polarized beam splitter (PBS) was introduced as shown in Fig.1 (b). The object light is split into two polarized beams with the PBS: one beam goes into the WFS and is used to detect the distortion; the other is corrected by the LCWFC and then goes to the imaging camera. With this configuration, the polarization energy loss is avoided[16-18]. But, the WFS and the LCWFC is parallel and the correction error of the LCWFC can't be detected by the WFS. Therefore, the whole system should be operated in open loop control[19-21]. It is difficult to use conventional deformable mirror in open loop control due to its hysteretic and nonlinearity properties. But for LCWFC, it has been proven to be a very high-precision corrector for generating a desired wavefront, which is very suitable for open loop control.

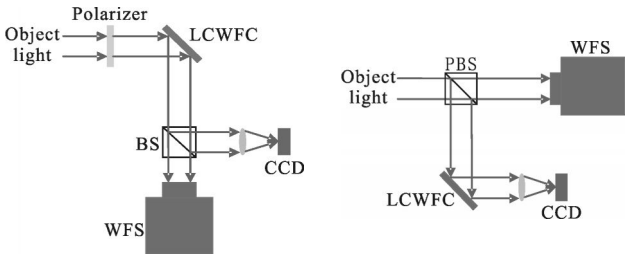

(a) Closed loop (b) Open loop

Fig.1 Optical configuration of the LC AOS

2 Spectral range expansion method with multi-LCWFCS

2.1 Waveband expansion scheme

Theoretically, LCWFC is only suitable to be used for

wavefront correction for a single wavelength and not on a waveband due to chromatism. However, if a minor error is allowed, LCWFC can be used to correct the distortion in a narrow spectral range. To fulfill this purpose, the chromatism effect on the correction accuracy of LCWFC should be analyzed. The chromatism of LCWFC includes refractive index chromatism and quantization chromatism. Refractive index chromatism is caused by the LC material and is generally called dispersion. Meanwhile, the quantization chromatism is caused by modulo 2π of phase wrapping[22-23]. Using the phase wrapping method, an LCWFC with the phase modulation of 2π can produce several, even tens of microns modulation magnitude and this is very suitable and essential in correcting atmospheric turbulence.

To analyze the dispersion of the LC material, the birefringence Δn was measured using a spectroscopic ellipsometer (JOBIN YVON) as shown in Fig.2[24]. In this instance, we are trying to achieve a broadband correction with an acceptable variation of of Δn. Since a phase wrapping technique is used, the phase distribution should be modulo 2π, and it should then be quantized [23]. Assuming that the quantization wavelength is λ_0, the thickness of the LC layer is d, and V_{max} denotes the voltage needed to obtain a 2π phase modulation, and then the maximum phase modulation of the LCWFC can be expressed as[24]:

$$\Delta\varphi_{max}(\lambda_0)=2\pi\frac{\Delta n(\lambda_0, V_{max})d}{\lambda_0}=2\pi \quad (1)$$

For any other wavelength λ, it can be rewritten as[24]:

$$\Delta\varphi_{max}(\lambda)=2\pi\frac{\Delta n(\lambda, V_{max})d}{\lambda} \quad (2)$$

From Eq.(2), we can see that the phase modulation error will be generated due to the variations of Δn and λ. For quantization wavelength of 550 nm, 633 nm and 750 nm, the variation of maximum phase modulation as a function of wavelength is shown in Fig.3. Assuming the deviation of the phase modulation is 0.1, for λ_0=550, 633 and 750 nm, the corresponding spectral ranges were calculated as 520-590 nm, 590-690 nm and 690-810 nm, respectively. If a 10% phase modulation error is acceptable, then the LCWFC only can be used to correct the distortion for a finite spectral range.

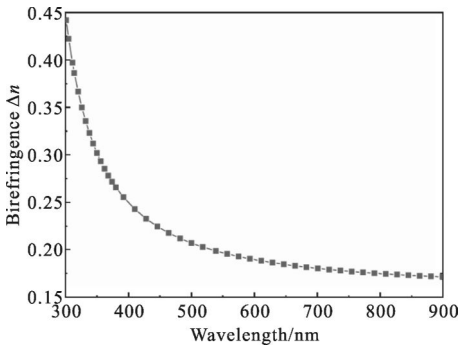

Fig.2 Birefringence Δn as a function of wavelength, measured by a spectroscopic ellipsometer

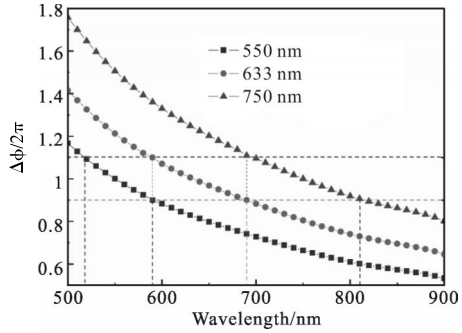

Fig.3 Phase modulation as a function of wavelength for λ_0=550 nm, 633 nm, and 750 nm, respectively; two horizontal dashed lines indicate the phase deviation range; while the four vertical dashed lines illustrate three sub-wavebands of 520-590 nm, 590-690 nm and 690-820 nm, respectively

The variation of Δn and λ affects the diffraction efficiency of the LCWFC. Using the Fresnel phase lens model, the diffraction efficiency for any other wavelength λ can be described as[25]:

$$\eta=\left|\frac{\sin(\pi d\Delta n(\lambda, V_{max})/\lambda)}{\pi(d\Delta n(\lambda, V_{max})/\lambda-1)}\right|^2 \quad (3)$$

The effects of Δn and λ on the diffraction efficiency are shown in Fig.4. For λ_0 = 550 nm, 633 nm, and 750 nm and their respective corresponding wavebands of 520-590 nm, 590-690 nm, and 690-810 nm, the maximum energy loss is 3%, which is acceptable for the LC AOS.

The above calculated results show that it is possible to correct the distortion in a narrow waveband using only one LCWFC. Therefore, to realize the distortion

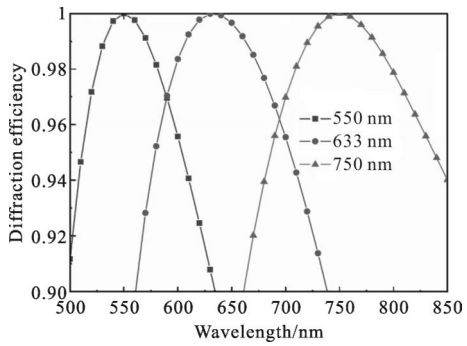

Fig.4 Diffraction efficiency as a function of wavelength for λ_0=550 nm, 633 nm, and 750 nm, respectively

correction in a broadband of 520−810 nm, three LCWFCs are necessary; each LCWFC is responsible for the correction of different wavebands and then three corrected beams are combined to realize the correction in the whole waveband. Figure 5 shows the optical setup for the broadband correction. Three dichroic beam splitters (DBSs) are used to acquire different wavebands. To solve the polarization dependence of the LCWFC, a PBS is used to split the unpolarized light into two linear polarized beams. Of course, this LC AOS must be operated with open loop control.

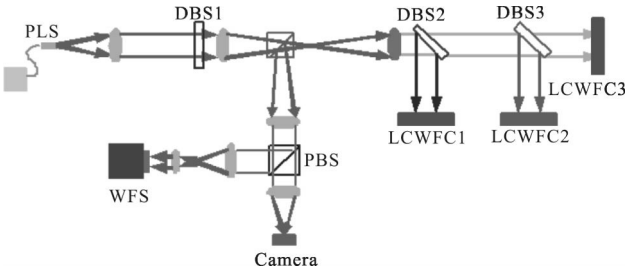

Fig.5 Optical set-up for broadband correction; PLS represents a point light source, PBS is a polarized beam splitter, DBS means dichroic beam splitter, DBS1 is a bandpass filter, and DBS2 and DBS3 are long-pass filters

2.2 Experimental results

In order to validate our method, a broadband correction experiment was performed with two LCWFCs based on open-loop control and the detailed information is illustrated in Ref.24. Compared with the optical layout in Fig.5, the LCWFC3 was removed from the experimental set−up (Fig.6), and a white light outputting from a fiber bundle was used as a point light source. Owing to computer limitation, only two LCWFCs were used to correct the distortions with the sub-wavebands of 520 − 590 nm and 590−690 nm. Both LCWFCs have an aperture of 7.68 mm × 7.68 mm, 512 pixels × 512 pixels, and a 200 Hz switching frequency. The WFS consists of 400 microlenses and has a 3 mm aperture; it also has a 500 Hz acquisition frequency. A US Air Force (USAF) resolution target was used to evaluate the correction effects in a broad waveband.

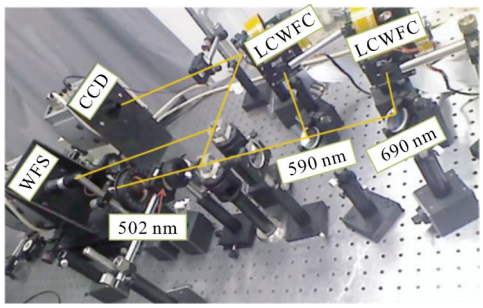

Fig.6 Optical layout for waveband of 520−690 nm correction with two LCWFCs

Firstly, the waveband of 520−590 nm was selected to perform the adaptive correction, then 590 −690 nm waveband, and at last, the combined waveband 520−690 nm. Figure 7 (a) shows the images of the resolution target without correction and Fig.7 (b)−(d) give the corrected results for different wavebands. All the images in Fig.7(a)−(d) have the same brightness due to the adjustment in the exposure time of the CCD camera. Actually, because imaging waveband of Fig. 7(d) is much wider than others, the image in Fig.7(d) has higher brightness than the others with the same exposure time. To observe the brightness change clearly, the intensity distribution on a line of the two - dimensional image is plotted in Fig.7(e). The measured data show that the intensity of 520 −690 nm is equal to the sum of 520−590 nm and 590−690 nm. Hence, the combined beam scheme may improve the imaging energy. Furthermore, as Fig.7 (c) and (d) have the same resolution, it can be seen that the correction resolution of wider waveband and two LCWFCs is the same as that of the narrow waveband and one LCWFC. Therefore, it can be said that our method is effective in extending the

waveband and improving the energy utilization ratio of the LC AOS.

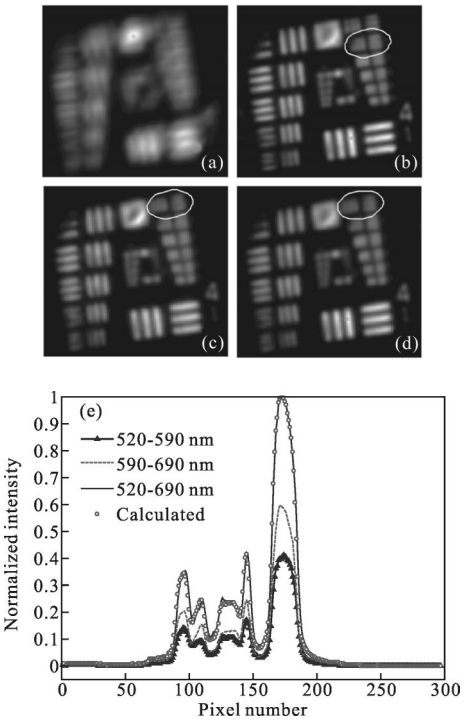

Fig.7 Images of the resolution target and the brightness distribution for different wavebands: (a) No correction; (b) 520−590 nm; (c) 590−690 nm; (d) 520−690 nm; the circular area represents the resolving limitation. (e) Brightness distribution in a line of the image

3 Optimal energy-splitting method

In the above work, we have demonstrated a PBS method to avoid the polarized energy loss and a multi-LCWFCs method to expand the spectral range. However, when a PBS is used, both the WFS and the imaging camera occupy half of the object light; this half/half energy splitting cannot be changed. Actually, to observe the weak object, the energy used for wavefront detection and imaging needs to be optimized. To obtain a suitable energy split, the energy detecting capability of the S – H WFS and the imaging camera will be analyzed firstly. The two underlying assumptions are that whole received energy is E and that the WFS and imaging cameras occupy respective halves of the whole energy. According to the Nyquist-Shannon sampling theory, 2×2 pixels are used to resolve the diffraction limit of the telescope. The received energy of the imaging camera can be rewritten as[26]:

$$E_{\mathrm{CCD}}=\frac{E}{8\pi}\left(\frac{r_0}{D}\right)^2 \tag{4}$$

here r_0 is the atmospheric turbulence coherence length, D represents the telescope aperture.

To the S-H WFS, assuming the optical disc of each microlens occupies 2×2 pixels to calculate the centroid, the received energy for one pixel of the S-H WFS can be computed by[26]:

$$E_{\mathrm{WFS}}=\frac{E}{2\pi}\left(\frac{r_0}{D}\right)^2 \tag{5}$$

Considering the exposure time of the camera, the energy ratio of the S-H WFS to the whole energy can be expressed as[26]:

$$R_{\mathrm{WFS}}=\frac{t_{\mathrm{CCD}}}{4t_{\mathrm{WFS}}+t_{\mathrm{CCD}}} \tag{6}$$

here t_{CCD} and t_{WFS} are the exposure times for the imaging camera and the S-H WFS respectively.

If 1 ms exposure time of S-H WFS is selected, R_{WFS} as a function of the exposure time of the imaging camera is shown in Fig.8. The received energy of the S-H WFS is approximately 70% with T_{CCD}=10 ms.

To capture the image of a star, an exposure time of tens of milliseconds is acceptable. Thus, according to the above analysis, more energy can be used to detect wavefront distortion. Assuming that T_{CCD} =10 ms, 70% energy can be allocated for the S-H WFS, and 30% energy can be used to perform imaging. To realize this, a waveband-splitting method is demonstrated as a replacement for the PBS method and the optical

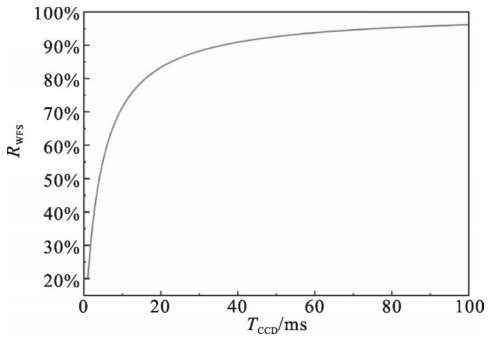

Fig.8 R_{WFS} as a function of the exposure time of the imaging camera with T_{WFS}=1 ms

configuration is shown in Fig.9. The object light is collimated using lens L1 and is then split into two beams using a long-wave pass filter (LWPF) in such a way that the beam with the short waveband is reflected toward the WFS, and the other beam with the long waveband passes through the LWPF and is zoomed using L2 and L3. Therefore, the energy occupied by the WFS can be adjusted easily by changing the 50% cutoff point of the LWPF. The PBS is placed in front of the LC WFC to split the unpolarized light into two linearly polarized beams. Thus, each polarized beam is directed toward the corresponding LC WFC, and the energy loss attributed to polarization dependence is avoided.

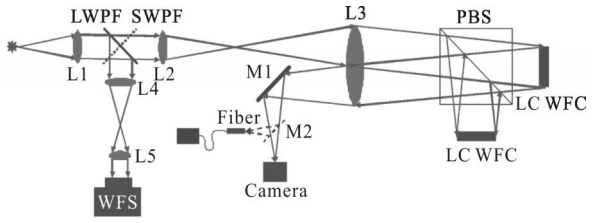

Fig.9 Optical layout for open-loop LC AOS with waveband-splitting method

To compare with the PBS method, the signal-to-noise ratios (SNRs) of the imaging camera and the S-H WFS are measured [27]. In the test configuration, the S-H WFS contained an EM CCD camera (DU860, Andor). The imaging camera was also an EM CCD camera (DV897, Andor), the sensitivity of which is equal to that of DU860. Firstly, the SNRs are measured for PBS method as shown in Fig.10 (a). It is shown that the difference between the SNR of the imaging camera and that of the S-H WFS is enlarged with the increased intensity. Furthermore, the SNR of the WFS is always less than that of the imaging camera. When the SNR of the WFS is 5, the SNR of the imaging camera is 9. This relationship indicates that the energy used for the imaging camera is superfluous and that more energy should be distributed to the WFS when a weaker object is detected. A suitable energy-splitting scheme is one wherein each used pixel receives the same amount of energy for both the imaging and the WFS camera. At this condition, both the imaging camera and the WFS can work normally. The variation in the SNR is measured for the waveband-splitting method as shown in Fig.10 (b). It indicates that the SNR of the WFS is almost equal to that of the imaging camera, whereas the normalized intensity increases gradually. Therefore, the used pixels of the imaging camera and the WFS have the same energy. These results show that the energy is split reasonably by the waveband-splitting method.

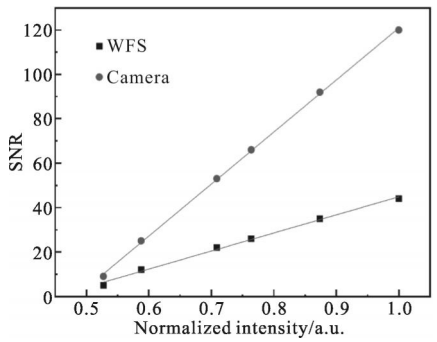

(a) PBS method

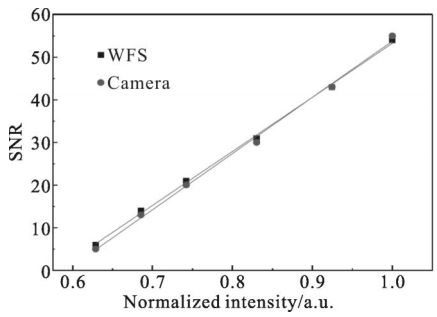

(b) Waveband-splitting method

Fig.10 SNR as a function of the normalized intensity

4 Adaptive corrections on the 1.2-meter telescope

Using optimal energy splitting method, an open-loop LC AOS was designed and constructed for a 1.2-meter telescope. Both LC WFCs (FP256, BNS) operated with 256×256 pixels at a 500 Hz frame rate. The S-H WFS had a 10 ×10 microlens array and a 930 Hz acquisition frequency. The imaging camera was also an EM CCD camera (DV897, Andor). The entire waveband was split into two sub-wavebands, namely, 350 nm to 700 nm and 700 nm to 950 nm, which were used to perform wavefront detection and imaging, respectively. This novel LC AOS was installed on a 1.2-meter telescope in June 2011.

An adaptive correction experiment was performed at nighttime on 19 June 2011. Before performing the correction, the Greenwood frequency and atmospheric coherence length were measured as 45 Hz and 7 cm, respectively. A star, SAO 9366 (4.45 visual magnitude), was selected as the observation object. The bandwidth of the LC AOS can reach up to 37 Hz. Figure 11 shows the image of SAO 9366 with and without adaptive correction. The blurry image changes to a small spot with the correction. Furthermore, after the correction, the angular resolution is 0.31″ which is 1.7 times the diffraction limit of the 1.2-meter telescope. An adaptive correction experiment was also performed to resolve a double star Diadem (α Com) which has an angular separation of 0.6″, and 4.85 and 5.53 visual magnitudes for two components respectively. The images of the double star with and without open-loop adaptive correction are shown in Fig.12. The two components of the double star are clearly resolved after correction.

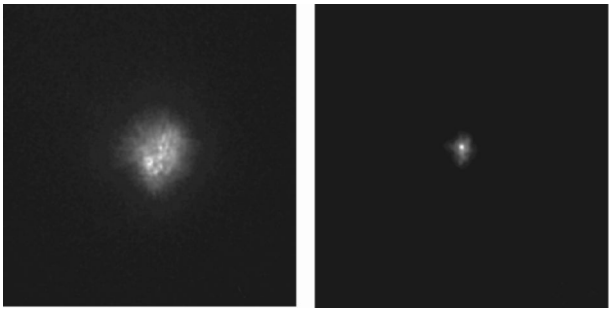

(a) Before correction (b) After correction

Fig.11 Images of the star SAO 9366

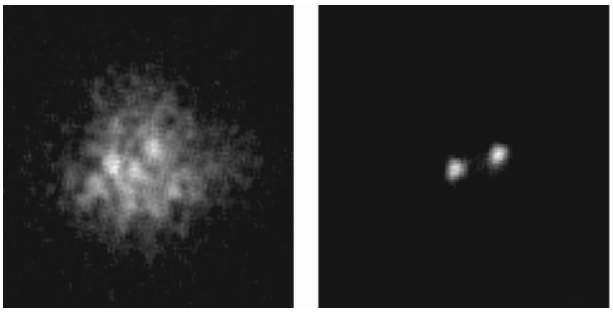

(a) Before correction (b) After correction

Fig.12 Images of the double star Diadem

5 Conclusions

In summary, based on open loop control, an optimal optical design is performed to improve the energy utilization ratio of the LC AOS. A PBS is used to solve the polarization dependence of the LCWFC. A waveband splitting method is utilized to expand the working waveband of the LC AOS. Finally, the energy utilization ratio of the LC AOS is improved and it may be used to observe the stars and the satellites. This system has been attached on the 1.2 m telescope at the CIOMP and some impressive observation results have been achieved.

References:

[1] Cao Z, Mu Q, Hu L, et al. Correction of horizontal turbulence with nematic liquid crystal wavefront corrector[J]. ***Opt Express***, 2008, 16: 7006-7013.

[2] Love G D. Wave-front correction and production of Zernike modes with a liquid-crystal spatial light modulator [J]. ***Appl Opt***, 1997, 36: 1517-1524.

[3] Restaino S, Dayton D, Browne S, et al. On the use of dual frequency nematic material for adaptive optics systems: first results of a closed-loop experiment [J]. ***Opt Express***, 2000, 6: 2-6.

[4] Neil M A A, Booth M J, Wilson T. Dynamic wave-front generation for the characterization and testing of optical systems[J]. ***Optics Letters***, 1998, 23: 1849-1851.

[5] Cao Z, Li X, Xuan L, et al. Recent progress in liquid crystal adaptive optics technique[J]. ***Chinese Optics***, 2012, 5 (1): 12-19. (in Chinese)

[6] Zheng X, Liu R, Xia M, et al. Retinal correction imaging system based on liquid crystal adaptive optics [J]. ***Chinese Optics***, 2014, 7(1): 98-104. (in Chinese)

[7] Burns D C, Underwood I, Gourlay J, et al. A 256×256 SRAM-XOR pixel ferroelectric liquid crystal over silicon spatial light modulator [J]. ***Optics Communications***, 1995, 119: 623-632.

[8] Peng Z, Liu Y, Cao Z, et al. Fast response property of low-viscosity difluorooxymethylene-bridged liquid crystals [J]. ***Liquid Crystals***, 2013, 40(1): 91-96.

[9] Peng Z, Liu Y, Yao L, et al. Improvement of the switching frequency of a liquid-crystal spatial light modulator with optimal cell gap[J]. ***Optics Letters***, 2011, 36(18): 3608-3610.

[10] Hu H, Hu L, Peng Z, et al. Advanced single-frame overdriving for liquid-crystal spatial light modulators [J].

Optics Letters, 2012, 37(16): 3324-3326.

[11] Love G D. Liquid crystal phase modulator for unpolarized light[J]. ***Appl Opt***, 1993, 32(13): 2222-2223.

[12] Love G D, Restaino S R, Carreras R C, et al. Polarization insensitive 127-segment liquid crystal wavefront corrector[C]// OSA Summer Topical Meeting on Adaptive Optics, 1996.

[13] Stockley J E, Sharp G D, Serati S A, et al. Analog optical phase modulator based on chiral smectic and polymer cholesteric liquid crystals[J]. ***Opt Lett***, 1995, 20: 2441-2443.

[14] Gu Naiting, Yang Zeping, Huang Linhai, et al. Measurement method of misalignment for Hartmann-Shack sensor and deformable mirror in adaptive optics system[J]. ***Infrared and Laser Engineering***, 2011, 40(2): 287-292. (in Chinese)

[15] Liu Ruixue, Zheng Xialiang, Xia Mingliang, et al. Accurate fixation of adaptive optics fundus imaging field of view based on visual target guidance [J]. ***Infrared and Laser Engineering***, 2015, 44(6): 1794-1799. (in Chinese)

[16] Mu Quanquan, Cao Zhaoliang, Li Dayu, et al. Open-loop correction of horizontal turbulence: system design and result [J]. ***Applied Optics***, 2008, 47(23): 4297-4301.

[17] Chen H, Xuan L, Hu L, et al. Optical design of miniaturization aberration correcting system for human eye[J]. ***Optics and Precision Engineering***, 2010, 18: 29-36. (in Chinese)

[18] Cheng Shaoyuan, Cao Zhaoliang, Hu Lifa, et al. Design of open loop liquid crystal adaptive optical system for 1 200 mm telescope[J]. ***Infrared and Laser Engineering***, 2010, 39 (2): 288-291. (in Chinese)

[19] Vogel C R, Yang Q. Modeling, simulation, and open-loop control of a continuous facesheet MEMS deformable mirror [J]. ***J Opt Soc Am A***, 2006, 23: 1074-1081.

[20] Blain C, Guyon O, Conan R, et al. Simple iterative method for open-loop control of MEMS deformable mirrors [C]// SPIE, 2008, 7015: 701534.

[21] Guzman D, Guesalaga A, Myers R, et al. Deformable mirror controller for open-loop adaptive optics [C]//SPIE, 2008, 7015: 70153X.

[22] Thibos L N, Bradley A. Use of liquid-crystal adaptive-optics to alter the refractive state of the eye [J]. ***Optometry and Vision Science***, 1997, 74: 581-587.

[23] Cao Z, Xuan L, Hu L, et al. Investigation of optical testing with a phase-only liquid crystal spatial light modulator[J]. ***Opt Express***, 2005, 13: 1059-1065.

[24] Mu Q, Cao Z, Hu L, et al. Novel spectral range expansion method for liquid crystal adaptive optics [J]. ***Optics Express***, 2010, 18(21): 21687-21696.

[25] Laude V. Twisted nematic liquid-crystal pixelated active lens [J]. ***Optics Communications***, 1998, 153: 134-152.

[26] Cao Z, Mu Q, Hu L, et al. Optimal energy-splitting method for an open-loop liquid crystal adaptive optics system [J]. ***Opt Express***, 2012, 20: 19331-19342.

[27] Xia M, Li C, Liu Z, et al. Adaptive threhold section method for Shack-Hartmann wavefront sensor[J]. ***Optics and Precision Engineering***, 2010, 18: 334-340. (in Chinese)